

2 – 8 KEV X-RAY NUMBER COUNTS DETERMINED FROM CHANDRA BLANK FIELD OBSERVATIONS

L. L. COWIE,¹ G. P. GARMIRE,² M. W. BAUTZ,³ A. J. BARGER,^{4,5,1} W. N. BRANDT,² A. E. HORNSCHMEIER²

The Astrophysical Journal Letters in press.

ABSTRACT

We present the 2 – 8 keV number counts from the 1 Ms *Chandra* observation of the *Chandra* Deep Field North (CDF-N). We combine these with the number counts from a 78 ks exposure of the Hawaii Survey Field SSA22 and with the number counts obtained in independent analyses of the CDF-S and the Hawaii Survey Field SSA13 to determine the number counts from 2×10^{-16} to 10^{-13} erg cm⁻² s⁻¹. Over this flux range the contribution to the X-ray background is 1.1×10^{-11} erg cm⁻² s⁻¹ deg⁻². When the contributions above 10^{-13} erg cm⁻² s⁻¹ from *BeppoSAX* or *ASCA* observations are included, the total rises to 1.4×10^{-11} erg cm⁻² s⁻¹ deg⁻². However, there appears to be substantial field-to-field variation in the counts in excess of the statistical uncertainties. When the statistical and flux calibration uncertainties (in both the background and source measurements) are taken into account, as much as 0.5×10^{-11} erg cm⁻² s⁻¹ deg⁻² could still be present in an unresolved component.

Subject headings: cosmology: observations — galaxies: distances and redshifts — galaxies: evolution — galaxies: formation — galaxies: active — galaxies: starburst

1. INTRODUCTION

The X-ray background (XRB) was the first cosmic background detected (Giacconi et al. 1962) and has been extensively characterized (Fabian & Barcons 1992). Its photon intensity $P(E)$, where E is the photon energy in keV and $P(E)$ has units [photons cm⁻² s⁻¹ keV⁻¹ sr⁻¹], can be approximated in the 1 – 15 keV range by $P(E) = AE^{-\Gamma}$ where $\Gamma \simeq 1.4$ (e.g., Marshall et al. 1980; Gendreau et al. 1995; Chen, Fabian, & Gendreau 1997). However, the XRB normalization is still somewhat uncertain with values in the 2 – 8 keV band lying between 1.3×10^{-11} (Marshall et al. 1980) and 1.8×10^{-11} erg cm⁻² s⁻¹ deg⁻² (Vecchi et al. 1999).

After the discovery of the XRB there was controversy over whether it arose from a superposition of discrete sources or from thermal bremsstrahlung from a hot intergalactic gas (e.g., Field 1972). We now know that the XRB cannot originate in an uniform hot intergalactic medium since the absence of a strong Compton distortion in the cosmic microwave background spectrum puts a stringent upper limit ($\sim 10^{-4}$) on such a contribution (Wright et al. 1994). However, there may be other sources of hard X-ray photons (e.g., Abazajian, Fuller, & Tucker 2001) which could contribute to the XRB without producing a Compton distortion, so constraining any residual diffuse background is of considerable interest.

The sources contributing the bulk of the 2 – 8 keV XRB were not found prior to the launch of the *Chandra X-ray Observatory*. While the soft (0.5 – 2 keV) background was largely resolved into sources by the *ROSAT* satellite (Hasinger et al. 1998), the spectra were too steep to account for the flat XRB spectrum. With the launch of

Chandra and the *XMM-Newton Observatory* the situation has evolved rapidly. Early 100 – 300 ks *Chandra* observations determined the number counts in the 2 – 8 keV band above 10^{-15} erg cm⁻² s⁻¹ (Mushotzky et al. 2000; Giacconi et al. 2001; Tozzi et al. 2001) and resolved the majority of the 2 – 8 keV XRB. Hasinger et al. (2001) have reported parallel results with *XMM-Newton*. Now the two 1 Ms *Chandra* exposures of the CDF-N (Brandt et al. 2001, hereafter B01) and the *Chandra* Deep Field South (CDF-S; Giacconi et al. 2002, hereafter G02; Campana et al. 2001, hereafter C01) have extended the counts to 2×10^{-16} erg cm⁻² s⁻¹. However, there is considerable spread (about 40%) in the normalizations, with the counts in the SSA13 (Mushotzky et al. 2000) and CDF-N (B01) fields being higher than the CDF-S counts (G02; C01) and the *XMM-Newton* Lockman Hole counts (Hasinger et al. 2001).

Here we provide a more detailed analysis of the number counts in the CDF-N, modelling the effects of Eddington bias and incompleteness. We also analyze a new 78 ks observation of the SSA22 field. We combine our counts with those measured by Mushotzky et al. (2000) from the 100 ks observation of the SSA13 field and those measured by C01 from the 1 Ms observation of the CDF-S to average over a spread of fields. We are currently analyzing the latter two fields using the same methods described here (L.L. Cowie et al., in preparation), but we note that similar number counts have been obtained for the CDF-S using very different methods (G02; C01).

We break with the tradition of X-ray number counts by using differential and not cumulative counts. Differential counts have many advantages in the statistical independence of the data points and in the ease with which breaks

¹Institute for Astronomy, University of Hawaii, 2680 Woodlawn Drive, Honolulu, HI 96822

²Department of Astronomy & Astrophysics, 525 Davey Laboratory, The Pennsylvania State University, University Park, PA 16802

³Center for Space Research, Massachusetts Institute of Technology, Cambridge, MA 02139

⁴Department of Astronomy, University of Wisconsin-Madison, 475 North Charter Street, Madison, WI 53706

⁵Department of Physics and Astronomy, University of Hawaii, 2505 Correa Road, Honolulu, HI 96822

and shape changes may be seen (c.f., Jauncey 1975).

2. X-RAY DATA

The observations of the CDF-N are presented in B01, where the 2 – 8 keV image and the exposure map are described. We follow B01 and use 2 – 8 keV fluxes since there is little sensitivity above 8 keV in the data. When we use the data of other authors, we convert to this band using consistent assumptions for the spectral index.

An important issue is the choice of spectrum for converting counts to flux. B01 converted using the Γ value determined from the ratio of the hard to soft band counts for each individual source. Others have converted using a single Γ chosen to match the expected average spectrum of the sources. G02 and C01 used $\Gamma = 1.4$, corresponding to the shape of the XRB, while Mushotzky et al. (2000) and Barger et al. (2001) used $\Gamma = 1.2$, based on the argument that the average spectra at these fluxes must be slightly harder than that of the XRB once allowance is made for the contribution of brighter sources (which, on average, are softer than the XRB). None of these methods is fully satisfactory for individual sources whose spectra may be more complex than a simple power-law. We adopt the $\Gamma = 1.2$ method which should give the best *average* conversion and hence the best estimate of the contribution of the sources to the XRB. This Γ , together with the $N_H = 1.6 \times 10^{20} \text{ cm}^{-2}$ of Galactic absorption, gives a conversion of counts to flux of $2.19 \times 10^{-11} \text{ erg cm}^{-2}$ for the charge transfer inefficiency corrected images of B01. The $\Gamma = 1.4$ conversion would reduce the fluxes by 4%, while use of individual Γ s would increase them by 13%. In combining the new counts with published number counts, we have applied the appropriate conversion.

There are various techniques for source selection, including sliding cells, wavelet based algorithms (B01; C01), and the optimal matched filter method (Vikhlinin et al. 1995). In the present analysis we use a matched aperture, which consists of a circular aperture of specified diameter and a background subtraction region which is an annulus 2 – 3 times the aperture radius. We determined the background from a cleaned image in which all known sources were masked out with artificial noise appropriate to the local exposure time. The background-subtracted source counts were determined by centering apertures on each pixel in the image and finding the local maxima. In each case if there was a secondary maximum within $2''$ of the primary, we combined the two sources. We determined the average background per aperture and selected only sources whose background-subtracted counts lay above the level where Poisson noise in the average background within the apertures would provide a probability of one false detection in the area.

We first analyzed the central area of the CDF-N image lying within $2.5'$ of the optical axis. Here we used a $2''$ aperture selected to optimize the recovery (based on the Monte Carlo simulations described below). This gave an average number of background counts of 1.8 per aperture; thus, we selected sources with background-subtracted counts lying above 9.0. We next analyzed the $6.5'$ radius area around the optical axis (including the previously analyzed $2.5'$ area) using a $4''$ diameter aperture and selected sources with background-subtracted counts above 14.7. The regions have fairly uniform ex-

posure times, which justifies the use of the average background. However, to test this, and also to check that the interchip regions, where the properties of the sources might be unusual, were not affecting the counts, we reran the search, clipping out the regions with lower exposure times. This had no significant effect on the number counts.

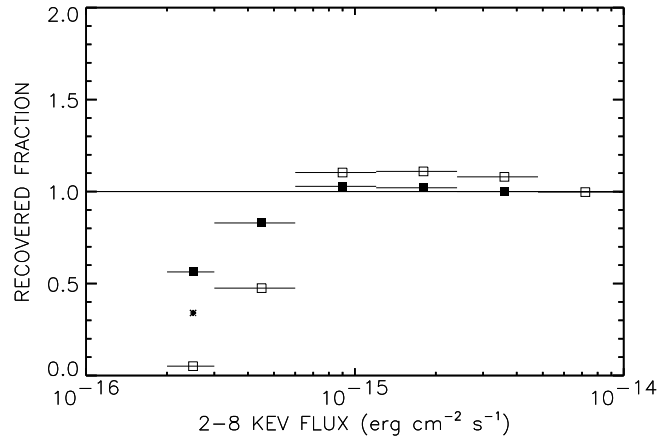


FIG. 1.— The ratio of the measured number counts to the input number counts in the $2.5'$ radius (solid boxes) and $6.5'$ radius (open boxes) regions. The width of each bin is shown by the short horizontal lines. Vertical error bars are smaller than the filled symbols. At high fluxes the retrieved counts precisely match the input counts. At intermediate fluxes Eddington bias becomes important and the retrieved number of sources exceeds the input counts. In the lowest flux bins, source recovery becomes incomplete. The star shows the recovered fraction in the $6.5'$ region times the relative area of the two regions.

We used the source counts determined in the $4''$ diameter aperture, with the subtracted background determined in the $8'' - 12''$ annulus, to get the fluxes of our sample. These counts were converted to count rates using the B01 exposure map. We determined the enclosed energy correction by measuring the ratio of the counts in a $20''$ diameter aperture relative to the $4''$ diameter aperture for all sources with fluxes above $10^{-15} \text{ erg cm}^{-2} \text{ s}^{-1}$ and fitting this with a third order polynomial as a function of the off-axis radius. There are no extended sources included in this computation. The enclosed energy correction agrees well with the standard ACIS PSF correction.

The flux calibration was tested by comparing the detected sources with the B01 catalog converted to $\Gamma = 1.2$. Above a flux limit of $3.5 \times 10^{-16} \text{ erg cm}^{-2} \text{ s}^{-1}$, the sample within the $6.5'$ radius region contains 152 sources and B01 141, of which 134 are common. For the sources in the B01 catalog above $5 \times 10^{-16} \text{ erg cm}^{-2} \text{ s}^{-1}$, the mean fluxes agree to 1% and the dispersion of the fluxes, when multiple sources are excluded, is 8%. Number counts generated from the two catalogs are nearly indistinguishable above this flux. At fainter fluxes the catalogs become more disjoint, reflecting the different source selection procedures, but the fluxes of the overlapping sample continue to agree.

The effects of incompleteness and bias were measured using Monte Carlo simulations in which a number of model X-ray images were created with noise properties matching that of the 1 Ms field and with sources drawn from parameterized descriptions of the number counts. 100 such images were generated and analyzed in the same way as the

actual X-ray image of the 1 Ms field. The artificial images were generated by masking all known sources from the real 1 Ms image and substituting artificial noise. Sources were then randomly drawn from the number counts model and added to this artificial image. To match the point spread function (PSF) the template sources were drawn from the brightest source in the real 1 Ms image in a $1'$ width annulus centered on the input position. This template was background-subtracted and flux-scaled to produce the correct input flux. The source identification and cataloging procedures were now run on the artificial image to generate the output counts. The output counts averaged over the 100 simulations were then compared with the input counts to determine the recovered fraction, which could then be used to correct the measured number counts. The input number counts model was next adjusted to match the observed number counts and the process repeated. The recovered fractions are shown in Figure 1 and illustrate the effect of Eddington bias (the recovered sources are brightened, which causes the observed counts to be high at intermediate fluxes) and the effect of incompleteness in the recovery at the lowest fluxes.

For fluxes between 2×10^{-16} and 3×10^{-16} erg cm $^{-2}$ s $^{-1}$, we used the $2.5'$ radius sample and its corrected area. Between 3×10^{-16} and 5×10^{-15} erg cm $^{-2}$ s $^{-1}$, we used the $6.5'$ sample and its corrected area. Above 5×10^{-15} erg cm $^{-2}$ s $^{-1}$, we used the entire CDF-N area lying within $10'$ of the optical axis, an area of 294 square arcminutes. At these large off-axis angles, simulations are not straightforward because of the complex PSFs which arise from the multiple positions and roll angles at which the data were taken. Here the fluxes were taken from the B01 catalog (converted to $\Gamma = 1.2$), which carefully calculated the total counts for the bright objects. The incompleteness and bias corrections were determined by comparing the raw number counts with those in the $6.5'$ radius region. 5×10^{-15} erg cm $^{-2}$ s $^{-1}$ lies well above the flux at which such effects become significant.

The 78 ks SSA22 field was analyzed using the standard reduction tools. A complete list of sources lying in the S2 and S3 chips and their fluxes were generated with WAVDETECT, using the assumptions of the present paper. More details can be found in M. W. Bautz et al., in preparation. The total area used was 0.035 square degrees. Only sources lying above 6×10^{-15} erg cm $^{-2}$ s $^{-1}$ (above which incompleteness and bias corrections are small) are included in the present analysis.

3. NUMBER COUNTS

We combined the fields by forming a total list of sources and determining the combined incompleteness and bias-corrected areas sampled at each flux. For the CDF-S we included the entire sample from C01, while for the SSA13 counts from Mushotzky et al. (2000) we restricted ourselves to sources with fluxes above 4×10^{-15} erg cm $^{-2}$ s $^{-1}$ to avoid any issues of bias and incompleteness which might be present at lower fluxes. The final sample consists of 373 sources with fluxes between 2×10^{-16} and 1.3×10^{-13} erg cm $^{-2}$ s $^{-1}$. The total corrected area ranges from 40 square arcminutes at the faint flux end to 0.25 square degrees at bright fluxes. The differential counts are the sum of the inverse areas of the sources in the flux

interval ΔS divided by the width:

$$n(S) = \frac{\sum(1/A_i)}{\Delta S} \quad (1)$$

We have normalized to a unit flux of 10^{-15} erg cm $^{-2}$ s $^{-1}$. In Fig. 2 we present the differential number counts per square degree per unit flux (filled squares) with 1σ uncertainties from the Poisson error in the number of sources. We also show the number counts from only the CDF-N and Hawaii fields (open triangles) and the CDF-S counts from C01 (open diamonds). There is a substantial difference between these two determinations of the number counts at fluxes below 10^{-15} erg cm $^{-2}$ s $^{-1}$. This difference could reflect the different methods of analysis (indeed, it occurs at fluxes where modelling corrections are required); however, all the methods of analysis so far applied to the fields have shown these same differences (B01; Giacconi et al. 2001b; C01), and it appears more probable that they result from field-to-field variations.

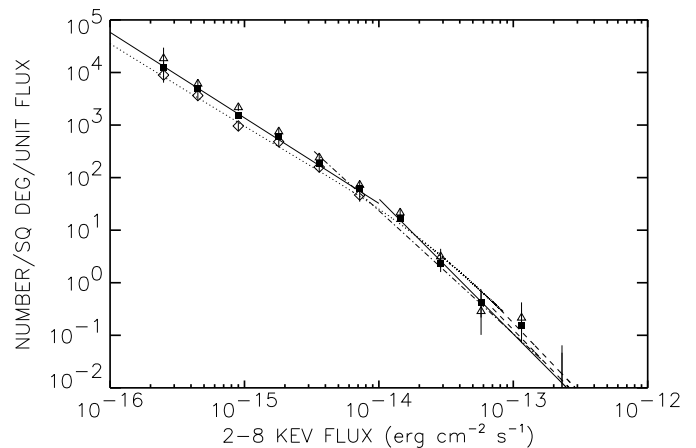


FIG. 2.— The combined differential counts from the four fields (solid boxes) with 1σ uncertainties. The y-axis units are relative to a unit flux of 10^{-15} erg cm $^{-2}$ s $^{-1}$. The open diamonds show the C01 CDF-S counts, and the open triangles show the combined CDF-N, SSA22, and SSA13 counts. The solid lines show the power-law fits to the composite counts over the flux ranges above and below 10^{-14} erg cm $^{-2}$ s $^{-1}$, while the dashed lines show the *ASCA* counts of della Cecca et al. (2000) and the *BeppoSAX* counts of Giommi et al. (2000). The dot-dash line shows Baldi et al. (2001)'s fit to their *XMM-Newton* counts. The dotted line shows C01's fit to the CDF-S and *ASCA* data.

The number counts cannot be fit by a single power-law but are well fit by a broken power-law. An area weighted maximum likelihood fit to the counts from all four fields, utilizing the bias-corrected areas (Murdoch, Crawford, & Jauncey 1973) gives a fit above 10^{-14} erg cm $^{-2}$ s $^{-1}$ of

$$n(S) = (39 \pm 5) \times (S/10^{-14})^{-2.57 \pm 0.22} \quad (2)$$

and below 10^{-14} erg cm $^{-2}$ s $^{-1}$ of

$$n(S) = (32 \pm 2) \times (S/10^{-14})^{-1.63 \pm 0.05}. \quad (3)$$

The normalizations are determined by matching the total number of objects in each range, and the uncertainties are 1σ . The units of $n(S)$ are number per square degree per 10^{-15} erg cm $^{-2}$ s $^{-1}$. The two power-laws intercept at a flux of 1.2×10^{-14} erg cm $^{-2}$ s $^{-1}$. A fit with the uncorrected areas gives a slightly steeper slope at the faint

end, consistent with the analytic expectation when uncorrected areas are used instead of bias-corrected areas (e.g., Schmitt and Maccacaro 1986). Fitting to only the CDF-N+Hawaii field counts gives a similar faint end slope (-1.61 ± 0.06) but higher normalization (45 ± 4), which, on integration, closely matches the cumulative 2 – 8 keV counts of B01, C01, using only the CDF-S data and force fitting the bright end of the flux counts to the *ASCA* slope, inferred a faint flux slope of -1.58 ± 0.03 and a break point of 1.7×10^{-14} erg cm $^{-2}$ s $^{-1}$ (the dotted line in Fig. 2). A systematic effect which could change the slope is the progressive hardening of the sources as the flux drops. The median Γ in B01 drops from 1.4 at 10^{-14} erg cm $^{-2}$ s $^{-1}$ to 0.9 at the faintest fluxes. Using these Γ s to compute the flux conversion increases the faint end slope to -1.68 .

Cross calibration is a concern in comparing with counts from other satellites. Tests using a point source common to *ASCA* and *Chandra* give agreement at about the 10% level for these satellites (Barger et al. (2001)) A more detailed analysis has recently been given by Snowden et al. (2001) who found that the *XMM* and *Chandra* ACIS-S3 data agree to about 5% in the 2 – 10 keV band and that the *ASCA* and *Chandra* fluxes agree to about 10%. The bright counts presented here match extremely well to the counts obtained by Baldi et al. (2001) using *XMM-Newton* (dash-dot line in Fig. 2) and lie only slightly below the *ASCA* counts of Ueda et al. (1999) and della Ceca et al. (2000) and the *BeppoSAX* counts of Giommi et al. (2000) (dashed lines in Fig. 2).

4. DISCUSSION

Fig. 3 shows the contribution to the XRB versus flux. The peak contribution arises near the break at 1.4×10^{-14} erg cm $^{-2}$ s $^{-1}$. The total contribution is 1.1×10^{-11} erg cm $^{-2}$ s $^{-1}$ deg $^{-2}$ over the flux range 2×10^{-16} to 10^{-13} erg cm $^{-2}$ s $^{-1}$. Extrapolating the power-law fit would add a further 0.2×10^{-11} erg cm $^{-2}$ s $^{-1}$ deg $^{-2}$ above 10^{-13} erg cm $^{-2}$ s $^{-1}$, similar to the value obtained from the *BeppoSAX* number counts. Use of the highest *ASCA* counts would only increase this to 0.3×10^{-11} erg cm $^{-2}$ s $^{-1}$ deg $^{-2}$. Extrapolating the faint end flux counts below 2×10^{-16} erg cm $^{-2}$ s $^{-1}$ would add 0.2×10^{-11} erg cm $^{-2}$ s $^{-1}$ deg $^{-2}$ to the total. For the *HEAO-1* normalization the observed contribution from sources above 2×10^{-16} erg cm $^{-2}$ s $^{-1}$ exceeds the background, while for the *BeppoSAX* and *ASCA* normalizations it is approximately 80% of the XRB. This would rise to 90% if we include the extrapolated faint end flux contribution.

The field-to-field differences can clearly be seen in Fig. 3, with the CDF-S and SSA22 lying below the CDF-N and SSA13. Between 2×10^{-16} and 10^{-14} erg cm $^{-2}$ s $^{-1}$ the CDF-N contributes 0.81×10^{-11} erg cm $^{-2}$ s $^{-1}$ deg $^{-2}$, while the CDF-S contributes 0.54×10^{-11} . This 40% difference is substantially above the Poisson noise expected from the number of sources.

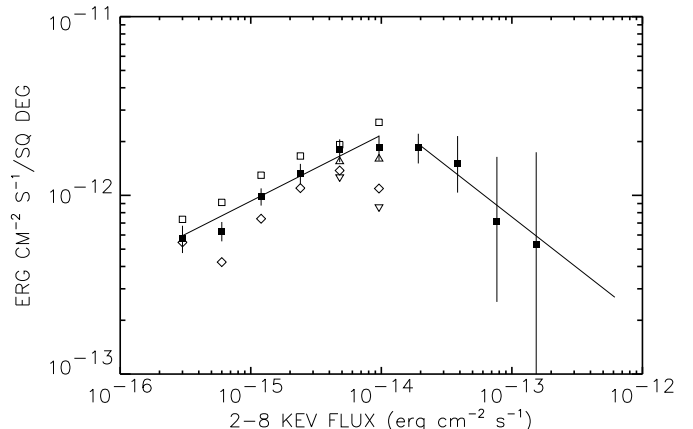


FIG. 3.— The contribution to the XRB versus flux. The solid boxes are the measured values in the combined sample. The lines show the values from the power-law fits. The open boxes show the CDF-N, the open diamonds the CDF-S, the open upward pointing triangles the SSA13 field, and the open downward pointing triangles the SSA22 field. The individual fields are shown only below 10^{-14} erg cm $^{-2}$ s $^{-1}$ where the error bars are small.

Given these variations and the uncertainties in the flux calibration of both the counts and the background, we estimate the minimum contribution of the resolved sources to the XRB to be 1.3×10^{-11} erg cm $^{-2}$ s $^{-1}$ deg $^{-2}$. Comparing this number to the maximum measured value of the XRB, 1.8×10^{-11} erg cm $^{-2}$ s $^{-1}$ deg $^{-2}$ (Vecchi et al. 1999), we find a maximum residual of 0.5×10^{-11} erg cm $^{-2}$ s $^{-1}$ deg $^{-2}$. The true value of any diffuse component is likely to be considerably lower.

We thank Sergio Campana for supplying the data on the CDF-S. Support came from NASA grant DF1-2001X (LLC, PI), NSF grant AST-0084816 (LLC), NASA grant NAS 8-38252 (GPG, PI), University of Wisconsin Research Committee funds granted by the Wisconsin Alumni Research Foundation (AJB), NSF grant AST-0084847 (AJB), NSF CAREER award AST-9983783 (WNB), NASA GSRP grant NGT 5-50247 (AEH), and the Pennsylvania Space Grant Consortium (AEH).

REFERENCES

- Abazajian, K., Fuller, G. M., & Tucker, W. 2001, *ApJ*, 562, 593
 Baldi, A., Molendi, S., Comastri, A., Fiore, F., Matt, G. & Vignali, C. 2001, *ApJ*, in press (astro-ph/0108514)
 Barger, A. J., Cowie, L. L., Mushotzky, R. F., & Richards, E. A. 2001, *AJ*, 121, 662
 Brandt, W.N., et al. 2001, *AJ*, 122, 2810 (B01)
 Campana, S., Moretti, A., Lazatti, D., & Tagliaferri, G. 2001, *ApJ*, 560, L65 (C01)
 Chen, L.-W., Fabian, A. C., & Gendreau, K. C. 1997, *MNRAS*, 285, 449
 della Ceca, R., Braitto, V., Cagnoni, I., & Maccacaro, T. 2001 *Mem. SAI* in press, (astro-ph/0007430)
 Fabian, A. C. & Barcons, X. 1992, *ARA&A*, 30, 429
 Field, G. B. 1972, *ARA&A*, 10, 227
 Gendreau, K.C., et al. 1995, *PASJ*, 47, L5
 Giacconi, R., Gursky, H., Paolini, F. R., & Rossi, B. B. 1962, *Phys. Rev. Lett.*, 9, 439
 Giacconi, R., et al. 2001a, *ApJ*, 551, 624
 Giacconi, R., et al. 2002, *ApJS*, in press (astro-ph/0112184) (G02)
 Giommi, P., Perri, M., & Fiore, F. 2000, *A&A*, 362, 799
 Hasinger, G., Burg, R., Giacconi, R., Hartner, G., Schmidt, M., Trumper, J., & Zamorani, G. 1998, *A&A*, 329, 482
 Hasinger, G., et al. 2001, *A&A*, 365, L45
 Jauncey, D. L. 1975, *ARA&A*, 13, 23
 Marshall, F., et al. 1980, *AJ*, 235, 4
 Murdoch, H. S., Crawford, D. F., & Jauncey, D. 1973, *ApJ*, 183, 1
 Mushotzky, R. F., Cowie, L. L., Barger, A. J., & Arnaud, K. A. 2000, *Nature*, 404, 459

- Schmitt, J. H. M. M. & Maccacaro, T. 1986, ApJ, 310, 334
Snowden, S., et al. 2001, <http://xmm.gsfc.nasa.gov/docs/xmm/estec2001/cf>
Tozzi, P., et al. 2001, ApJ, 562, 42
Ueda, Y., et al. 1999, ApJ, 518, 656
- Vecchi, A., Molendi, S., Guainazzi, M., Fiore, F., & Parmar, A.N. 1999, A&A, 349, L73
Vikhlinin, A., Forman, W., Jones, C., & Murray, S., 1995, ApJ, 451, 542
Wright, E. L. et al. 1994, ApJ, 420, 450